Analysis and design of the taper in metal-grating periodic slow-wave structures for rectangular Cerenkov masers*

Chen Ye(陈 晔)[a)b)†], Zhao Ding(赵 鼎)[a)], Wang Yong(王 勇)[a)], and Shu Wen(舒 雯)[a)b)]

[a)] *Key Laboratory of High Power Microwave Sources and Technologies, Institute of Electronics, Chinese Academy of Sciences, Beijing* 100190, *China*

[b)] *Graduate University of Chinese Academy of Sciences, Beijing* 100049, *China*

(Received 27 September 2011; revised manuscript received 4 November 2011)

The hybrid-mode dispersion equation of the metal-grating periodic slow-wave structure for a rectangular Cerenkov maser is derived by using the Borgnis function and field-matching methods. An equivalent-circuit model for the taper of the groove depth that matches the smooth waveguide to the metal-grating structure is proposed. By using the equivalent-circuit method, as well as the Ansoft high frequency structure simulator (HFSS) code, an appropriate electromagnetic mode for beam-wave interaction is selected and the equivalent-circuit analysis on the taper is given. The calculated results show that a cumulative reflection coefficient of 0.025 for the beam-wave interaction structure at a working frequency of 78.1 GHz can be reached by designing the exponential taper with a TE_{z10} rectangular waveguide mode as the input and the desired TE_{x10} mode as the output. It is worth pointing out that by using the equivalent-circuit method, the complex field-matching problems from the traditional field-theory method for taper design can be avoided, so the taper analysis process is markedly simplified.

Keywords: rectangular Cerenkov maser, Borgnis function method, equivalent-circuit method, HFSS, taper

PACS: 84.40.Ik, 94.05.Pt, 41.60.Bq **DOI:** 10.1088/1674-1056/21/5/058401

1. Introduction

Cerenkov radiation occurs when the electron velocity is greater than the phase velocity of an electromagnetic wave in a slow-wave structure, in which the electromagnetic wave could be exponentially amplified because of beam-wave coupling. The Cerenkov maser, characterized by high power and high frequency coherent radiation, has become one of the most promising candidates for producing millimeter-wave and microwave in the fields of plasma heating, linear accelerators, communication systems, and radars.

The traditional Cerenkov maser adopts a cylindrical waveguide as the interaction structure, where the annular electron beam interacts with the TM_{on} mode. Since the 1950s, a series of achievements have been made with the Cerenkov maser.[1−7] However, to retain a proper shape and position of the beam for beam-wave interaction, and to avoid beam deformation and the boundary interception of the beam resulting from the high current density in the hollow beam, a strong axial magnetic field must be applied, which commonly needs large focusing equipment.[8] Moreover, the geometric scale of the practical device is always analogous with the working wavelength, so the operation for high power levels is limited when the wavelength becomes short.[9] Hence, since the early 1990s, considerable attention has been paid to a novel Cerenkov maser, a rectangular Cerenkov maser (RCM), in which a sheet electron beam interacts with a loaded dielectric layer or metal periodic slow-wave structure (SWS). Compared with the cylindrical Cerenkov maser, the focusing equipment in the RCM is much smaller, and the output power of the device can be further enhanced.

The metal-grating SWS is commonly used as the interaction structure of the RCM for beam-wave interaction. Compared with the interaction structure with a loaded dielectric layer, the structural damage resulting from the dielectric boundary interception of the electron beam and the breakdown of the electric field can be avoided where the high power level operation can be improved. Moreover, the shape and the

*Project supported by the National Natural Science Foundation of China (Grant No. 60801031).

†Corresponding author. E-mail: chenye07@mails.gucas.ac.cn

© 2012 Chinese Physical Society and IOP Publishing Ltd

geometric scale of the metal-grating structure are easier to control in practice. However, to avoid reflecting oscillation induced by the changes in the boundary conditions at two ends of the metal-grating structure, a taper for matching the smooth waveguide to the metal-grating structure must be applied. Theoretical and experimental results on SWS and taper design have been reported since the 1950s.[10−15] McVey *et al.*[1] analyzed the taper that matched the smooth waveguide to the metal-grating structure with minimal reflection based on the coupled mode theory, and discussed the reflection characteristics of different piecewise-linear tapers. The coupled mode equations were solved for a dielectric taper by using the field-theory method in Ref. [2], in which the TE_{z10} mode was properly coupled to the desired EH_{10} hybrid slow-wave mode.

In the present paper, the hybrid-mode dispersion equation of the metal-grating SWS for the RCM is derived using the Borgnis potential function. By using the equivalent-circuit method, the taper of the groove depth in the metal-grating SWS is analysed, and the numerical results are compared with those obtained from the Ansoft HFSS code. The mode transition from the TE_{z10} mode to the TE_{x10} slow-wave mode for beam-wave interaction is realized through optimally designing an exponential taper with the objective of minimal reflection.

2. Dispersion equation

Figure 1 shows a three-dimensional (3D) model of the metal-grating SWS for the RCM, which consists of a rectangular waveguide with height p and width w, and periodic metal-gratings. The grating has a periodicity d, groove width s and depth h. By choosing the z-axis as the longitudinal direction, the modes in this structure are hybrid modes that simultaneously include the z-axial field components E_z and H_z, which can be represented by the superposition of the normal TE and TM modes in a perfect metal waveguide. However, as in Refs. [1] and [16], the hybrid mode discussed here can be simply expressed as a transverse electric mode along the x-direction, TE_x. As shown in Fig. 1, the whole interaction structure is divided into two field-regions. Regions 1 (above the metal-gratings) and 2 (inside the meal-gratings) are defined as the regions $0 < y < p - h$ and $-h < y < 0$, respectively. For the TE_x mode in the structure, the Borgnis potential functions can be expressed as $U^{(x)} = 0$, $V^{(x)} \neq 0$. By using the separation of variables method, the potential function V is represented as

$$V_1^{(x)} = \sum_{n=-N}^{N} A_n \sin k_x \left(x + \frac{w}{2}\right) \times \cosh \upsilon_n (p - h - y)\, \mathrm{e}^{\mathrm{j}\beta_n z}, \quad (1)$$

$$V_2^{(x)} = \sum_{m=0}^{+\infty} B_m \sin k_x \left(x + \frac{w}{2}\right) \times \cosh \upsilon_m (y + h) \cos k_m z, \quad (2)$$

where $\upsilon_n = \sqrt{\beta_n^2 + k_x^2 - k_0^2}$, $\upsilon_m = \sqrt{k_m^2 - k_0^2 + k_x^2}$, and $k_m = m\pi/s$, $m = 0, 1, 2 \ldots$.

According to the corresponding relationships between the Borgnis potential functions and the field components of the electromagnetic waves, H_x and E_z can be expressed by the superposition of the potential function U and V as

$$H_{x\mathrm{i}} = V_{\mathrm{i}}^{(x)} \quad (3)$$

and

$$E_{z\mathrm{i}} = \frac{-\mathrm{j}\omega\mu}{k_0^2 - k_x^2} \frac{\partial V_{\mathrm{i}}^{(x)}}{\partial y}. \quad (4)$$

By applying the continuity conditions of the tangential fields at the plane $y = 0$,

$$E_{z1}(x, 0^+, z) = \begin{cases} E_{z2}(x, 0, z), & 0 < z < s, \\ 0, & s < z < d, \end{cases} \quad (5)$$

$$H_{x1}(x, 0^+, z) = H_{x2}(x, 0^-, z). \quad (6)$$

The hybrid-mode dispersion equation of the metal-grating SWS can be obtained as

$$\mathrm{d}\nu_0 \tan h\,[\nu_0(p - h)] \left\{1 - \nu_x s \tan(\nu_x h) \times \sum_{n=0}^{+\infty} \frac{\sin c^2(\beta_n s/2)}{\mathrm{d}\nu_n \tan h[\nu_n(p - h)]}\right\} = 0, \quad (7)$$

where $\nu_0 = \sqrt{\beta^2 + k_x^2 - k_0^2}$ and $\nu_x = \sqrt{k_0^2 - k_x^2}$.

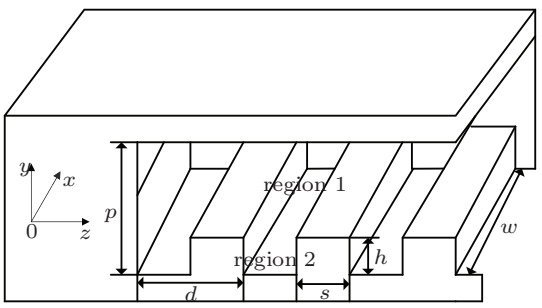


Fig. 1. 3D model of the metal-grating SWS.

3. Equivalent-circuit analysis of the groove-depth taper

3.1. Model

In order to avoid the reflecting oscillation resulting from the abrupt changes of the boundary conditions at two ends of the metal-grating structure, a taper that matches the smooth waveguide to the SWS must be applied. Figure 2 shows the geometrical model for the taper of the groove depth. The step discontinuity of the taper discussed in this paper is defined by the gradual change in groove depth. Hence, the taper can be divided into many metal-grating units with different groove depths and identical geometrical periodicity by the dashed lines, as shown in Fig. 2.

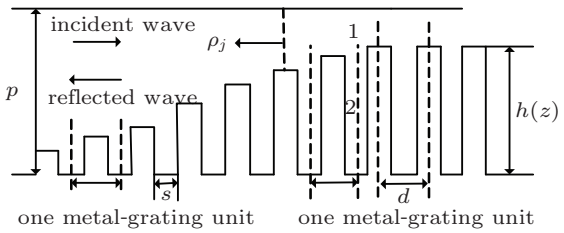


Fig. 2. Geometrical model for the groove-depth taper.

By using the equivalent-circuit method, region 1 in Fig. 2 (above the metal-gratings) can be considered as a parallel-surface transmission line with a characteristic impedance, Z_c per unit width, where $Z_c = Z_0$ $(p - h)$ with Z_0 denotes the characteristic impedance of the transmission line. Moreover, region 2 (inside the metal-gratings) is expressed as a short-circuited stub which connects in series with the main transmission line with a periodicity d, where $\mathrm{j}X$ represents the stub reactor and $\mathrm{j}X = \mathrm{j}Z_0 s \tan(\beta h)$.

Based on the analysis discussed above, the equivalent-circuit model of one metal-grating unit is shown in Fig. 3. Usually, this model is considered as a four-pole network. However, if the couplings to high-order modes in the taper are neglected, the model can be equivalently expressed as the cascade of three two-pole networks, i.e., a transmission line with electrical length $\theta/2$, a series reactance $\bar{X}$, and another transmission line with electrical length $\theta/2$, where $\theta = \beta d$, $\bar{X} = X/Z_c$. Based on this model, the reflection characteristic for the metal-grating structure can be analysed in detail.

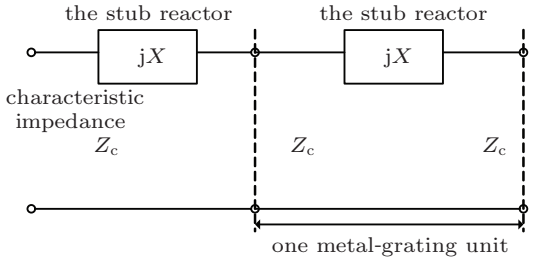


Fig. 3. Equivalent-circuit model of one metal-grating unit.

3.2. Reflection characteristics

The transmission matrix of the metal-grating unit in Fig. 3 can be obtained by calculating the continued product of the transfer matrixes of the two transmission lines and the series reactance in the equivalent-circuit model, as[17]

$$\begin{bmatrix} V_n \\ I_n \end{bmatrix} = \begin{bmatrix} \cos\theta - \dfrac{\bar{X}}{2}\sin\theta & \mathrm{j}\left(\sin\theta + \dfrac{\bar{X}}{2}\cos\theta + \dfrac{\bar{X}}{2}\right) \\ \mathrm{j}\left(\sin\theta + \dfrac{\bar{X}}{2}\cos\theta - \dfrac{\bar{X}}{2}\right) & \cos\theta - \dfrac{\bar{X}}{2}\sin\theta \end{bmatrix} \begin{bmatrix} V_{n+1} \\ I_{n+1} \end{bmatrix}. \tag{8}$$

Subsequently, by applying the continuity conditions of the voltage and current at the corresponding end-surfaces of two adjacent metal-grating units, the following relationships are obtained:[18]

$$V_{n+1} = \mathrm{e}^{-\mathrm{j}\beta d} V_n, \quad I_{n+1} = \mathrm{e}^{-\mathrm{j}\beta d} I_n, \tag{9}$$

where $\mathrm{j}\beta$ is the propagation constant and n denotes the sequence number of the metal-grating unit.

Combining formulas (8) and (9), the equations on propagation constant β, can be written as

$$(A - \mathrm{e}^{\mathrm{j}\beta d})V_{n+1} = -BI_{n+1},$$

and

$$-CV_{n+1} = (D - \mathrm{e}^{\mathrm{j}\beta d})I_{n+1}. \tag{10}$$

There exists a nonzero solution only if the determinant of coefficient for each equation in formula (10) is zero, hence the following relationship can be obtained

through algebraic operations:

$$\bar{Z}_B = \frac{V_{n+1}}{I_{n+1}} = \frac{2B}{D - A + \sqrt{(A+D)^2 - 4}}, \tag{11}$$

where $\bar{Z}_B$ represents the normalized characteristic impedance.

By substituting the corresponding matrix elements in formula (8) into expression (11), $\bar{Z}_B$ will be expressed as

$$\bar{Z}_B = \sqrt{\frac{2\sin\theta + \bar{X}\cos\theta + \bar{X}}{2\sin\theta + \bar{X}\cos\theta - \bar{X}}}. \tag{12}$$

Hence, the reflection coefficient at the position of abrupt groove-depth change is obtained as

$$\rho = \frac{\bar{Z}_B^2 - \bar{Z}_B^1}{\bar{Z}_B^2 + \bar{Z}_B^1}, \tag{13}$$

where $\bar{Z}_B^1$ and $\bar{Z}_B^2$ represent the characteristic impedances in the plane $z = 0$ for $z < 0$ and $z > 0$ directions, respectively.

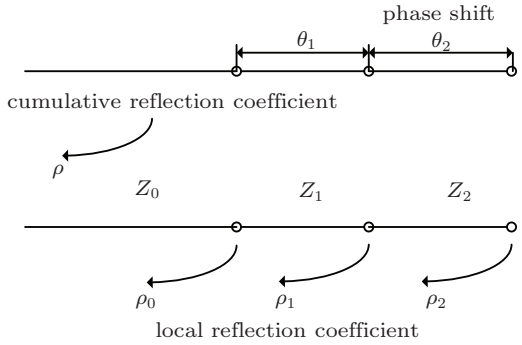


Fig. 4. The cumulative reflection coefficient and local reflection coefficient for the metal-grating structure.

According to small reflection theory, the cumulative reflection coefficient ρ_{T}, can be obtained by summing the contributions of the local reflection coefficients and transmission coefficients with appropriate phase shifts. If the multiple reflected waves are neglected in the calculation, ρ_{T} has the form of

$$\rho_{\mathrm{T}} = \rho_0 + \sum_j \rho_j \exp\left(\mathrm{i}2d\sum_j \beta^j\right), \tag{14}$$

where the subscript j indicates the position along the taper in units of geometrical periodicity (d), the reflection coefficient of each individual step (ρ_j) can be computed from formula (13), and $\exp(\mathrm{i}2d\beta^j)$ represents the corresponding phase shift for ρ_j.

4. Numerical calculation and simulation

As an example, an exponential taper that couples the TE_{z10} smooth waveguide mode to the TE_{x10} slow-wave mode will be designed based on the equivalent-circuit method discussed above, and the numerical results calculated from the formula (14) will be further verified by the Ansoft HFSS code in this section. All the structural parameters are listed in Table 1.

Table 1. Structural dimensions of the metal-grating structure for simulation calculations.

Parameters	Size/mm
d	0.5
s	0.25
h	0.61
p	2.1
w	2.5

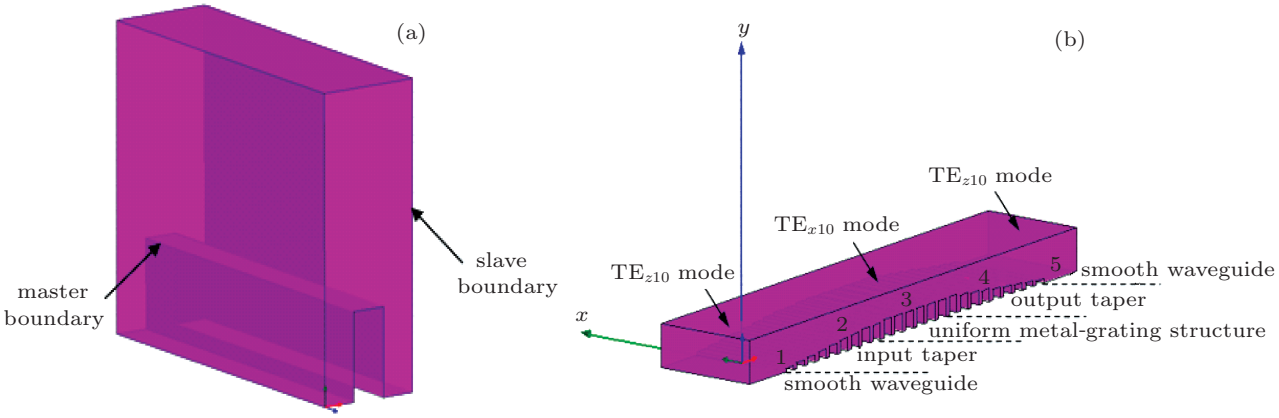


Fig. 5. (colour online) Simulation models for the metal-grating SWS. (a) Model of one metal-grating unit without taper, (b) model of the whole interaction structure with taper.

Figure 5(a) shows the simulation model of one metal-grating unit without taper, in which the inner part of this model is assigned to vacuum, and the master and slave boundaries for the simulation of periodic structures are set to be on the end-surfaces of the model. The whole metal-grating structure consists of many metal-grating units that are connected in series with each other. As an example, the operating point (synchronization point) for the beam-wave interaction is assumed to be located on the dispersion curve of the first harmonic wave in this paper. The Ansoft HFSS Eigen-mode solver is used in the calculation.

In Fig. 6, the horizontal axis represents phase delay, which is the product between the z-axis propagation constant and the geometrical periodicity of the metal-grating structure, and n denotes the harmonic order. The solid line in Fig. 6 denotes the dispersion curve of the lowest-order mode obtained from the Ansoft HFSS code, and the dashed line represents the result calculated from formula (7). The frequency characteristic of the normalized phase velocity for the first harmonic wave of the structure is shown in Fig. 7. Figure 8 shows the electric field intensity vector distribution at a working frequency of 78.1 GHz.

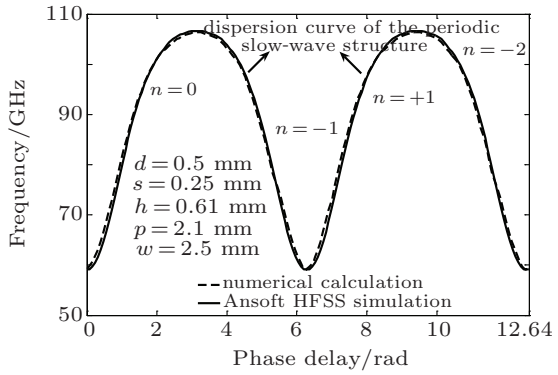


Fig. 6. Dispersion curves for the metal-grating structure.

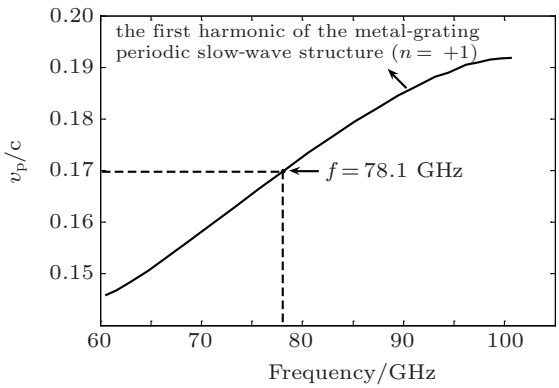


Fig. 7. Phase velocity versus working frequency for the first harmonic in the metal-grating SWS.

The electromagnetic mode that corresponds to the working frequency of 78.1 GHz is selected for the beam-wave interaction by observing the electric field intensity vector distributions at different working frequencies on the upper-surface of the metal-grating structure, and the frequency characteristic curve of the phase velocity. There are two possible reasons for the mode selection. First, the phase velocity of the electromagnetic wave in this mode, v_p, can be reduced to a value of $0.17c$ (c represents the light velocity, 3×10^8 m/s), which is necessary for the electromagnetic wave to keep pace with the electron beam and interact with the beam efficiently as shown in Fig. 7. Second, in terms of the polarization direction, the longitudinal (z-axis) change of the electric field intensity vector for this mode is dominant compared with the transverse change, which could strengthen the beam-wave coupling and further enhance the beam-wave interaction efficiency, as shown in Fig. 8.

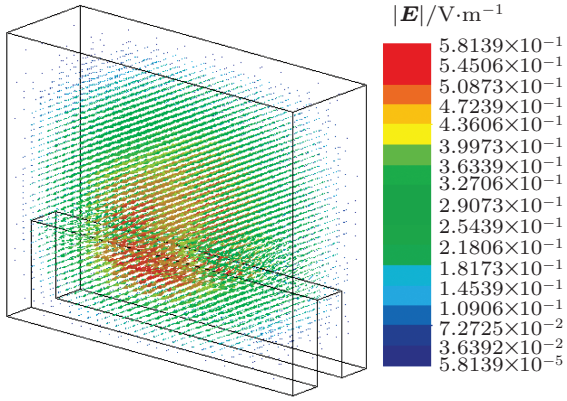


Fig. 8. (colour online) Electric field intensity vector ($\boldsymbol{E}$) distribution at a working frequency of 78.1 GHz.

Figure 5(b) shows the simulation model of the whole metal-grating structure with the input taper and the output taper. In Fig. 5(b), the model is divided into five sections, i.e., section 1 (-15 mm $< z <$ 0 mm), section 2 (0 mm $< z <$ 15 mm), section 3 (15 mm $< z <$ 30 mm), section 4 (30 mm $< z <$ 45 mm), and section 5 (45 mm $< z <$ 60 mm), which correspond to the input smooth waveguide, the input taper, the uniform metal-grating waveguide (the groove depth of the metal-grating units are all identical), the output taper, and the output smooth waveguide, respectively. The TE_{z10} mode is incident from the left end-face of section 1, where the longitudinally coupled field component E_z is almost zero. The values of the groove depth of different metal-grating units, h, vary exponentially with the positions along the z-axis

in section 2. The numbers of metal-grating units in sections 2, 3, and 4 are all 30. The length of each smooth waveguide in sections 1 and 5 is 15 mm. Other structural parameters are shown in Table 1.

Through optimally designing the groove depth of the metal-grating unit (h) when other relevant parameters are kept unchanged, with the objective of minimum reflection, the z-axis position-dependent relationship for h can be expressed as $h(z) = 1 - \exp(-0.0401jd)$, where j ($j = 0, 1, 2, \ldots$) and d represents the sequence number of the metal-grating units along the z-axis in section 2 and the geometrical periodicity of the metal-grating units, respectively. The driven-modal module of the Ansoft HFSS code is used in the following simulation.

Figure 9 shows the transverse field intensity distributions for the longitudinal coupled field component E_z at a working frequency of 78.1 GHz. As shown in Fig. 9, the amplitude of the field component E_z approaches the peak value around the upper-surface of the metal-grating structure and gradually deceases to zero along the y-axis. The amplitude of the E_z in section 1 is very close to zero, slowly increases in section 2, and finally reaches a certain stable value in section 3, as shown in Figs. 9(a)–9(d). This can be explained by the fact that the TE_{z10} mode of the smooth waveguide is gradually matched to the TE_{x10} mode of the uniform metal-grating structure that simultaneously includes the field components E_z and H_z, due to the contributions of the taper of groove depth in section 2. Likewise, the TE_{x10} mode can be converted into the TE_{z10} mode of the smooth waveguide when passing through the output taper in section 4, in which process the amplitude of the E_z gradually falls to zero as shown in Figs. 9(e) and 9(f). It should be noted that the taper of groove depth smoothly matches the TE_{z10} mode to the desired TE_{x10} mode, which can strengthen the energy exchange between the electron beam and the electromagnetic mode because the amplitude of the longitudinal coupled field component E_z is markedly increased.

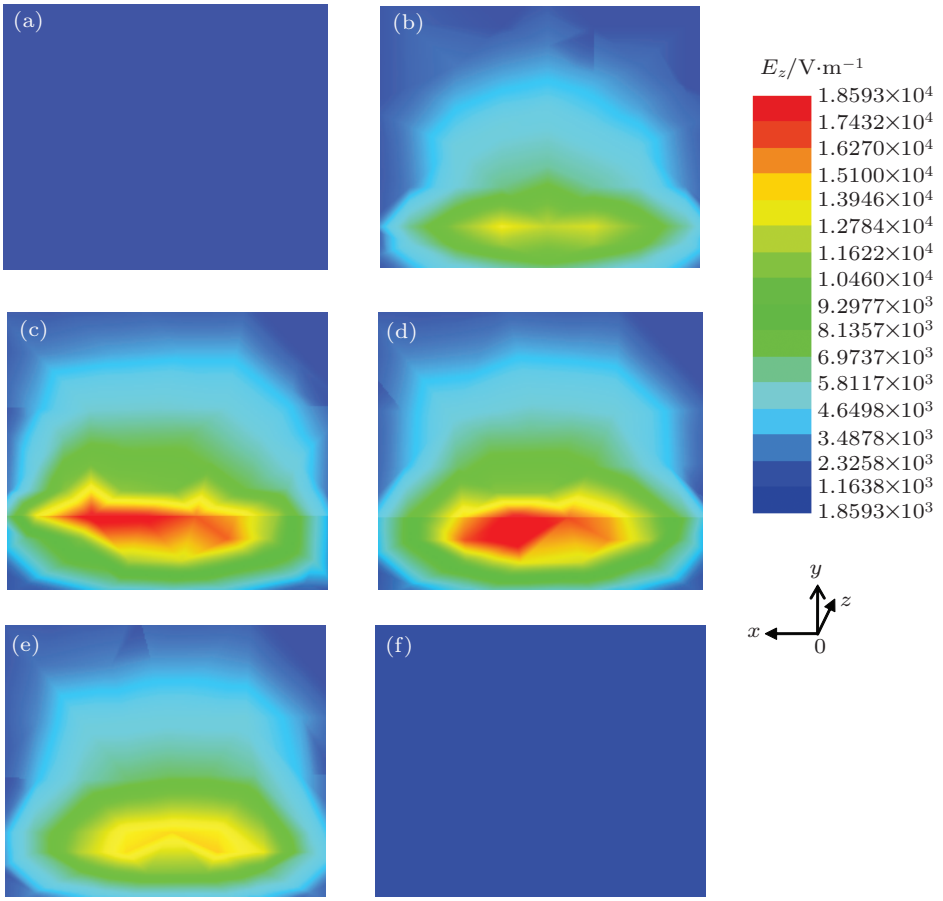


Fig. 9. (colour online) Field intensity distributions of the longitudinal coupled field (E_z) in different transverse sections at a working frequency of 78.1 GHz. (a) region 1, $z = -15$ mm, (b) region 2, $z = 11$ mm, (c) region 3, $z = 17$ mm, (d) region 3, $z = 27$ mm, (e) region 4, $z = 31.5$ mm, and (f) region 5, $z = 60$ mm.

Figure 10 shows the frequency characteristics of the cumulative reflection coefficient for the meal-grating structure with exponential tapers designed in this paper. The solid line represents the result calculated from formula (14) based on the equivalent-circuit method, and the dotted line corresponds to the result obtained from the Ansoft HFSS code. In Fig. 10, the reflection coefficient gradually rises with the increase in working frequency and this growth slows down when the frequency is above 77.8 GHz, and the reflection coefficient reaches a peak value around 0.026 at a frequency of 78.3 GHz and then falls down with a further increase in working frequency. As shown in Figs. 7, 8, and 10, by designing the exponential taper defined by the change in groove depth based on the equivalent-circuit method, the cumulative reflection coefficient can reach 0.025 at a working frequency of 78.1 GHz that corresponds to the transmission mode selected for the beam-wave interaction in this paper, which has a value of $0.17c$ for the phase velocity of the electromagnetic wave and a dominant longitudinal (z-axis) change in electric field intensity vector in the sense of the polarization direction.

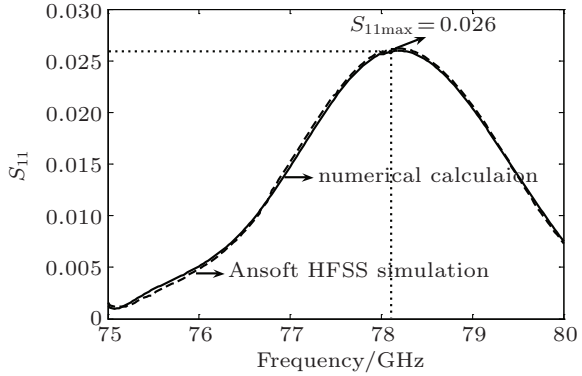


Fig. 10. Cumulative reflection coefficients S_{11} versus the working frequency for the metal-grating SWS.

5. Conclusion

The hybrid-mode dispersion equation of the metal-grating structure for RCM is derived by solving a 3D multi-region field-matching problem with the Borgnis potential functions. An equivalent-circuit model of the taper that matches the TE_{z10} mode of the smooth waveguide to the desired TE_{x10} mode of the metal-grating structure is proposed. The relevant numerical results are verified to be consistent with the results from the Ansoft HFSS code. It can be concluded that a cumulative reflection coefficient of 0.025 for the metal-grating structure at a working frequency of 78.1 GHz can be realized by designing the exponential taper with the TE_{z10} guide mode serving as the input and the TE_{x10} mode as the output based on the equivalent-circuit method. Moreover, the complex field matching problems of the traditional field-theory method can be avoided by using the equivalent-circuit method, which can be helpful for analysing and designing taper profiles in the future.

References

[1] McVey B D, Basten M A, Booske J H, Joe J and Scharer J E 1994 *IEEE Trans. Microwave Theory Tech.* **42** 995

[2] Sheng-Fuh R C, Scharer J E, and Booske J H 1992 *IEEE Trans. Plasma Sci.* **20** 293

[3] Zhao D, Ding Y, Wang Y and Ruan C J 2010 *Phys. Plasmas* **17** 113110

[4] He J, Wei Y Y, Gong Y B, Duan Z Y and Wang W X 2010 *Acta Phys. Sin.* **59** 2843 (in Chinese)

[5] Latsas G P, Moraitou M D, Ioannidis Z C and Tigelis I G 2010 *IEEE Trans. Plasma Sci.* **38** 1185

[6] Chaudhury A, Panda P C and Srivastava V 2011 *Proceedings of IEEE International Vacuum Electronics Conference*, Bangalore, February 21–24, 2011 p. 63

[7] Wu Y, Xu Z, Xu Y, Jin X, Chang A B, Li Z H, Huang H, Liu Z, Luo X, Ma Q S and Tang C X 2011 *Acta Phys. Sin.* **60** 196 (in Chinese)

[8] Shlapakovskii A S 1996 *Proc. SPIE* **2843** 137

[9] Chen Y, Zhao D and Wang Y 2011 *Chin. Phys.* B **20** 108402

[10] GongY B, Lu Z G, Wang G J, Wei Y Y, Huang M Z and Wang W X 2006 *J. Infrared Millim. Waves* **25** 173 (in Chinese)

[11] Lu Z G, Wei Y Y, Gong Y B and Wang W X 2006 *J. Infrared Millim. W.* **25** 349 (in Chinese)

[12] Hu Y L, Yang Z H, Li B, Li J Q, Huang T, Jin X L, Zhu X F and Liang X P 2010 *Acta Phys. Sin.* **59** 5439 (in Chinese)

[13] Peng W F, Hu Y L, Yang Z H, Li J Q, Lu Q R and Li B 2010 *Acta Phys. Sin.* **59** 8478 (in Chinese)

[14] Tang K S, Zhao G, Li S and Yin H J 2009 *J. Electronics Information Technology* **31** 736 (in Chinese)

[15] Jiao C Q and Luo J R 2007 *J. Electronics Information Technology* **29** 2010 (in Chinese)

[16] Zhang K and Li D 2001 *Electromagnetic Theory for Microwaves and Optoelectronics* 1st ed (Beijing: Electronics Industry Press) (in Chinese)

[17] David M Pozar 2006 *Microwave Engineering* (Beijing: Publishing House of Electronics Industry) (in Chinese)

[18] Collin R E 1981 *Foundation of Microwave Engineering* (Beijing: Posts and Telecommunications Press) (in Chinese)